Accepted to Phys. Fluids 10.1063/5.0147691

Scattering by source-type flows in disordered media

[a)]Gerardo SEVERINO[1] and Francesco GIANNINO[2]

[1]*Division of Water Resources Management*, University of Naples - FEDERICO II
via Universitá 100 - I80055, Portici (NA), ITALY (e-mail: gerardo.severino@unina.it)

[2]*Division of Ecology and System Dynamics*, University of Naples - FEDERICO II
via Universitá 100 - I80055, Portici (NA), ITALY (e-mail: francesco.giannino@unina.it)

(Dated: 11 April 2023)

Scattering through a natural porous formation (by far the most ubiquitous example of disordered medium) represents a formidable tool to identify effective flow and transport properties. In particular, we are interested here in the scattering of a passive scalar as determined by a steady velocity field which is generated by a line of singularity. The velocity undergoes erratic spatial variations, and concurrently the evolution of the scattering is conveniently described within a stochastic framework that regards the conductivity of the hosting medium as a stationary, Gaussian, random field. Unlike the similar problem in uniform (in the mean) flow-fields, the problem at stake results much more complex. Central to the present study is the fluctuation of the driving field, that is computed in closed (analytical) form as a large time limit of the same quantity in the unsteady state flow regime. The structure of the second-order moment X_{rr}, quantifying the scattering along the radial direction, is explained by the rapid change of the distance along which the velocities of two fluid particles become uncorrelated. Moreover, two approximate, analytical expressions are shown to be quite accurate in reproducing full simulations of X_{rr}. Finally, the same problem is encountered in other fields, belonging both to classical and to quantum physics. As such, our results lend themselves to being used within a context much wider than that exploited in the present study.

Keywords: source-type flow · scattering · stochastic modelling · radial moment

[a)] corresponding author

Accepted to Phys. Fluids 10.1063/5.0147691

INTRODUCTION AND PROBLEM FORMULATION

Scattering processes generated by source (typically well) type flows represent one of the most powerful tool to estimate flow and transport parameters of aquifers (Rubin, 2003). In reservoir engineering, quantitative interpretation of scattering in radial-type flows entails designing well completion, packer setting, and coring section. Moreover, in the search of oil and gas, the study of scattering is used as a tool for isopach mapping, as well as convergence mapping. The ultimate aim is to obtaining reservoir engineering data of equal (if not greater) reliability than those secured by core testing. This is particularly relevant in highly permeable reservoir formations (Tarek, 2018). In the theory of composites, the study of scattering of tracer particles in fluid-saturated porous media is relevant for chromatography, and catalysis (Milton, 2002).

In the present study, we are interested into scattering as generated by an injecting line-source embedded in a porous formation (FIG. 1). The medium is, as a rule in natural

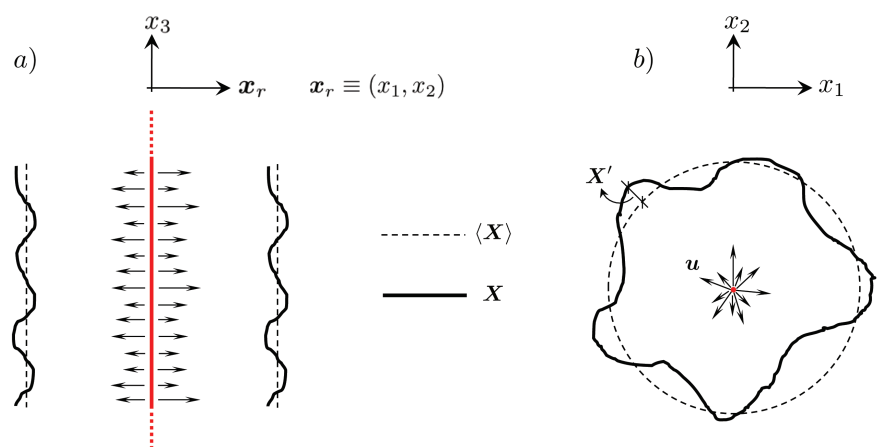

FIG. 1. Sketch of scattering in the vertical (a)-view) and planar (b)-view) section, as generated by a (red) line of singularity. Continuous (black) line represents the current particle front $\boldsymbol{X}$, whereas the dashed line refers to the mean front $\langle \boldsymbol{X} \rangle$. Moreover, $\boldsymbol{X}' = \boldsymbol{X} - \langle \boldsymbol{X} \rangle$ and $\boldsymbol{u}$ are the particle trajectory fluctuation and the velocity field, respectively.

formations, disordered (i.e. heterogeneous) with the conductivity K, in particular, changing erratically in the space by orders of magnitude. Such variability affects tremendously scattering, as demonstrated both theoretically (Koplik, Redner, and Hinch, 1994; Le Borgne, Dentz, and Carrera, 2008) and experimentally (Kurowski *et al.*, 1994). The approach to account for these variations, and to model the associated uncertainty, is to regard the log-conductivity $\ln K(\boldsymbol{x})$ as a stationary, Gaussian, random field. As a a consequence, the dependent flow and transport variables become stochastic, and we wish to characterize scattering by means of the first and second-order spatial moments:

$$\langle \boldsymbol{X}(t)\rangle = \boldsymbol{R}(t), \qquad \langle X'_m(t) X'_n(t)\rangle = X_{m,n}(t) \qquad m,n=1,2,3 \tag{1}$$

(hereafter $\langle\rangle$ shall denote the ensemble average operator). Before proceeding further, it is worth reminding that (1) is valid under the ergodic condition, the requirement that allows replacing spatial averages with their statistical ensembles. For the problem at stake, ergodicity is met provided that the length ℓ_w of the line is much larger than the vertical integral scale I_v of $\ln K$ (Dagan, 1989). Since $\ell_w \sim \mathcal{O}(1 \div 10\,m)$ and $I_v \sim \mathcal{O}(10^{-2} \div 1\,m)$, ergodicity is fulfilled in most of the real situations.

Thus, central for the study of scattering are the mean $\boldsymbol{R}$ and the fluctuation $\boldsymbol{X}' = \boldsymbol{X} - \boldsymbol{R}$ of the trajectory $\boldsymbol{X} \equiv \boldsymbol{X}(t)$ of a fluid particle (FIG. 1). Unlike scattering driven by mean uniform flows (an exhaustive overview can be found in Dagan, 1989), here computing the fluctuation $\boldsymbol{X}'$ is an extremely complex problem (see, e.g. Tartakovsky, Tartakovsky, and Meakin, 2008), due to the strong coupling of the velocity field $\boldsymbol{V}$ with the spatial variability of K. A simplification is achieved (for details, see Indelman and Rubin, 1996) by dealing with a medium characterized by $\sigma_Y^2 \ll 1$ (weakly heterogeneous formation), which leads to the following system of equations:

$$\begin{cases} \dot{\boldsymbol{R}} = \boldsymbol{U}(\boldsymbol{R}), & \boldsymbol{R}(0) = \boldsymbol{R}_0, \\ \dot{\boldsymbol{X}}' - \nabla \boldsymbol{U} \cdot \boldsymbol{X}' = \boldsymbol{u}(\boldsymbol{R}), & \boldsymbol{X}'(0) \equiv (0,0,0), \end{cases} \tag{2}$$

being $\boldsymbol{U} \equiv \langle \boldsymbol{V}\rangle$ and $\boldsymbol{u} = \boldsymbol{V} - \boldsymbol{U}$ the mean and the fluctuation of the velocity, respectively. In order to compute the latter, we start from the governing flow equation:

$$-\nabla \cdot [K(\boldsymbol{x}) \nabla H(\boldsymbol{x})] = \frac{\bar{Q}}{\langle K\rangle} K(0,0,x_3)\,\delta(\boldsymbol{x}_r), \qquad \lim_{x\to\infty} H(\boldsymbol{x}) = 0 \tag{3}$$

(Severino and Cuomo, 2020), where the specific energy (head) $H \equiv H(\boldsymbol{x})$ is related to the velocity $\boldsymbol{V}$ *via* the constitutive model $\boldsymbol{V} = -(K/n)\,\nabla H(\boldsymbol{x})$. The porosity n, in line with the experimental data (see, e.g. Rubin, 2003), is regarded as a given constant, whereas $\bar{Q}$ is the specific (per unit length) strength. We cast the mathematical problem (3) in dimensionless form by introducing the scaled coordinate $\boldsymbol{x}/\ell_c$, where the characteristic length-scale will be chosen later on. Hence, introduction of the normalized fluctuation $Y \equiv \ln(K/K_G)$ ($K_G \equiv \exp\langle \ln K\rangle$ is the geometric mean) transforms eq. (3) (for simplicity we keep the former notations) as follows:

$$-\nabla^2 H(\boldsymbol{x}) = Q\,\delta(\boldsymbol{x}_r) + \nabla Y(\boldsymbol{x}) \cdot \nabla H(\boldsymbol{x}), \qquad Q \equiv \frac{\bar{Q}}{\langle K\rangle\,\ell_c}, \tag{4}$$

where we have accounted for $K(0,0,x_3)\,\delta(\boldsymbol{x}_r) \equiv K(\boldsymbol{x})\,\delta(\boldsymbol{x}_r)$. Solving eq. (4) is a formidable and quite complex task, with no exact solution. As a matter of fact, one has to sort with approximate methods. In the present paper we adopt a strategy which ultimately leads to simple (analytical) results. More precisely, we expand the head into asymptotic series $H = H^{(0)} + H^{(1)} + \ldots$ of Y with $H^{(n)} = \mathcal{O}(Y^n)$, and substitute into (4) to get the governing equations for the leading-order term $H^{(0)}$ and the fluctuation $H^{(1)}$:

$$-\nabla^2 H^{(0)} = Q\,\delta(\boldsymbol{x}_r) \Rightarrow H^{(0)}(x_r) = -\frac{Q}{2\pi}\ln x_r, \quad -\nabla^2 H^{(1)}(\boldsymbol{x}) = \nabla_r H^{(0)}(x_r)\cdot\nabla_r Y(\boldsymbol{x}), \tag{5}$$

being $\nabla_r \equiv \left(\frac{\partial}{\partial x_1}, \frac{\partial}{\partial x_2}\right)$ the gradient in the horizontal plane. Once the second of (5) is solved, the mean $U = \langle V(x_r)\rangle$ and the fluctuation $\boldsymbol{u}$ of the velocity field are obtained upon expansion of the constitutive model, i.e.

$$U(x_r) = \frac{QK_G}{2\pi n x_r}, \qquad \boldsymbol{u}(\boldsymbol{x}) = U(x_r)\,Y(\boldsymbol{x}) - \left(\frac{K_G}{n}\right)\nabla H^{(1)}(\boldsymbol{x}). \tag{6}$$

Hence, the mean R and the fluctuation X' of the trajectory are computed by carrying out the quadrature in (2) with zero initial condition, i.e.

$$R(t) = \left(\frac{Qt}{n\pi}\right)^{1/2}, \qquad X'(R) = U(R)\int_0^R \mathrm{d}x_r\,\frac{u(x_r,\theta,0)}{U^2(x_r)} \tag{7}$$

(we have switched to R as independent variable, and taken ℓ_c/K_G as characteristic time scale). Moreover, since we are concerned with radial scattering, we have set $x_3 = 0$. The second-order moment X_{rr} writes as:

$$X_{rr}(R) = \left\langle X'^2\right\rangle = U^2(R)\int_0^R\int_0^R \mathrm{d}x'_r\,\mathrm{d}x''_r\,\frac{u_{rr}(x'_r,x''_r)}{U^2(x'_r)\,U^2(x''_r)}. \tag{8}$$

It is worth noting that the covariance $u_{rr}(x'_r,x''_r) \equiv \langle u(\boldsymbol{x}'_r)\,u(\boldsymbol{x}''_r)\rangle$ does not depend upon the anomaly θ, due to the axial symmetry of the mean flow, and it is obtained straightforwardly from the second of (6), the final result being:

$$u_{rr}\left(x_r', x_r''\right) = \sigma_Y^2\,\rho_Y\left(\left|\boldsymbol{x}_r' - \boldsymbol{x}_r''\right|\right) U\left(x_r'\right) U\left(x_r''\right) + \left(\frac{K_G}{n}\right)^2 \frac{\partial^2}{\partial x_r' \partial x_r''}\left\langle H^{(1)}\left(\boldsymbol{x}_r'\right) H^{(1)}\left(\boldsymbol{x}_r''\right)\right\rangle - \frac{K_G}{n}\left[U\left(x_r'\right)\frac{\partial}{\partial x_r''}\left\langle Y\left(\boldsymbol{x}_r'\right) H^{(1)}\left(\boldsymbol{x}_r''\right)\right\rangle + U\left(x_r''\right)\frac{\partial}{\partial x_r'}\left\langle H^{(1)}\left(\boldsymbol{x}_r'\right) Y\left(\boldsymbol{x}_r''\right)\right\rangle\right]. \tag{9}$$

Thus, central for the present study is the fluctuation $H^{(1)}$ that is derived as:

$$H^{(1)}\left(\boldsymbol{x}\right) = Q\int \mathrm{d}\bar{\boldsymbol{x}}\, G_3^{\infty}\left(\boldsymbol{x} - \bar{\boldsymbol{x}}\right)\frac{\partial Y\left(\bar{\boldsymbol{x}}\right)}{\partial \bar{x}_m}\frac{\partial G_2^{\infty}\left(\bar{\boldsymbol{x}}_r\right)}{\partial \bar{x}_m} \qquad (m = 1, 2) \tag{10}$$

(Fiori, Indelman, and Dagan, 1998), where

$$G_d^{\infty} \equiv \frac{1}{4\pi}\begin{cases} \ln x_r^{-2} & d = 2 \\ x^{-1} & d = 3 \end{cases} \tag{11}$$

is the d-dimensional steady Green function. Moreover, $\boldsymbol{x}_r$ and $\boldsymbol{x}$ represent the position in $\mathbb{R}^2$ and $\mathbb{R}^3$, respectively. It is convenient to write the head's fluctuation (10) as $H^{(1)}\left(\boldsymbol{x}\right) = Q/\left(2\pi\right)^{3/2}\int \mathrm{d}\boldsymbol{k}\tilde{Y}(\boldsymbol{k})\exp\left(-\jmath\boldsymbol{k}\cdot\boldsymbol{x}\right)\mathcal{H}\left(\boldsymbol{k}\right)$ with

$$\mathcal{H}\left(\boldsymbol{k}\right) = -\jmath k_m\int \mathrm{d}\bar{\boldsymbol{x}}\exp\left(-\jmath\boldsymbol{k}\cdot\bar{\boldsymbol{x}}\right) G_3^{\infty}\left(\bar{x}\right)\frac{\partial}{\partial \bar{x}_m} G_2^{\infty}\left(\left|\boldsymbol{x}_r - \bar{\boldsymbol{x}}_r\right|\right), \tag{12}$$

where the fluctuation Y has been written by means of its spectral (*Fourier transform*) representation $\tilde{Y}$, i.e.

$$Y(\boldsymbol{x}) = \int \frac{\mathrm{d}\boldsymbol{k}}{\left(2\pi\right)^{3/2}}\tilde{Y}\left(\boldsymbol{k}\right)\exp\left(-\jmath\boldsymbol{x}\cdot\boldsymbol{k}\right). \tag{13}$$

As it will be clearer later on, the analytical evaluation of the integral (12) enables one to express the head-covariance $\left\langle H^{(1)}\left(\boldsymbol{x}\right) H^{(1)}\left(\boldsymbol{y}\right)\right\rangle$ (and concurrently the velocity covariance u_{rr}) by means of only two quadratures, that are easily carried out once the shape of the spectrum is specified. Besides the tremendous reduction of the computational burden (Fiori, Indelman, and Dagan, 1998, expressed the same covariances via six quadratures), the analytical expression of $\mathcal{H} \equiv \mathcal{H}\left(\boldsymbol{k}\right)$ is also instrumental in the identification of the hydraulic properties from transport data (inverse problem). Finally, the same integral is found in other branches of the physics. In fact, in quantum mechanics it serves to infer the structure as well as the charge-density of particles (Martin and Shaw, 2019), whereas in electrodynamics the same integral is encountered when one aims at computing the electric field generated by a localized/distributed density of charges (Jackson, 2007). As a consequence, its evaluation finds application within a spectrum much wider than that exploited in the present study.

The remainder of the paper is organized as follows: we compute explicitly the integral (12). Then, we discuss the structure and the behavior of the flow variables related to it, before moving to the modelling of scattering through disordered (randomly heterogeneous) media. Finally, we end up with concluding remarks.

ANALYTICAL COMPUTATION OF $\mathcal{H}$

A direct computation of (12) does not seem achievable, unless one deals with particular structures of heterogeneity (Severino, 2011). For this reason we follow in the sequel a different avenue. More precisely, we start from the unsteady state version of the same flow problem, i.e.

$$\exp\left(-Y\right)\frac{\partial}{\partial t}G-\nabla^2 G-\nabla Y\cdot\nabla G=\delta(\boldsymbol{x}_r)\delta\left(t\right), \qquad G\left(\boldsymbol{x},0\right)=0, \tag{14}$$

and compute the integral (10) as $\lim_{t\to\infty}\int_0^t \mathrm{d}\tau\, G^{(1)}\left(\boldsymbol{x},\tau\right)$, by virtue of the *superposition principle*, being $G^{(1)}\equiv G^{(1)}\left(\boldsymbol{x},t\right)$ the first order approximation of (14). In particular, for a homogeneous medium ($Y\equiv 0$) one recovers from (14) the equation of the d-dimensional unsteady Green function, i.e. $G_d\left(\boldsymbol{x},t\right)=\left(4\pi t\right)^{-d/2}\exp\left[-|\boldsymbol{x}|^2/\left(4t\right)\right]$. In order to compute $G^{(1)}$, we procede like before. Thus, we expand G in the asymptotic series $G=G^{(0)}+G^{(1)}+\ldots$ with $G^{(n)}=\mathcal{O}\left(Y^n\right)$. Then, substitution into (14) and retaining the first order term provide the equation for the fluctuation $G^{(1)}$, i.e.

$$\frac{\partial}{\partial t}G^{(1)}-\nabla^2 G^{(1)}=Y\frac{\partial}{\partial t}G^{(0)}+\nabla Y\cdot\nabla G^{(0)}, \qquad G^{(0)}\equiv G_3. \tag{15}$$

To solve eq. (15), we apply Laplace transform over the time and Fourier transform (13) over the space. The final result, after employing integration by parts, reads as:

$$G^{(1)}(\boldsymbol{x},t)=-\int\frac{\mathrm{d}\boldsymbol{k}\,\tilde{Y}\left(\boldsymbol{k}\right)}{\left(2\pi\right)^{3/2}}\int_0^t\mathrm{d}\tau\int\mathrm{d}\bar{\boldsymbol{x}}\exp\left(-\jmath\,\boldsymbol{k}\cdot\bar{\boldsymbol{x}}\right)\left[\delta\left(\bar{\boldsymbol{x}}_r\right)\delta\left(\tau\right)G_3\left(|\boldsymbol{x}-\bar{\boldsymbol{x}}|,t-\tau\right)-\right.$$
$$\left.\frac{\partial}{\partial\bar{x}_m}G_3\left(|\boldsymbol{x}-\bar{\boldsymbol{x}}|,t-\tau\right)\frac{\partial}{\partial\bar{x}_m}G_2(\bar{x}_r,\tau)\right]=\jmath k_m\int\frac{\mathrm{d}\boldsymbol{k}\,\tilde{Y}\left(\boldsymbol{k}\right)}{\left(2\pi\right)^{3/2}}\int_0^t\mathrm{d}\tau\int\mathrm{d}\bar{\boldsymbol{x}}\exp\left(-\jmath\,\boldsymbol{k}\cdot\bar{\boldsymbol{x}}\right)\times$$
$$G_3\left(|\boldsymbol{x}-\bar{\boldsymbol{x}}|,t-\tau\right)\frac{\partial}{\partial\bar{x}_m}G_2(\bar{x}_r,\tau) \qquad (m=1,2)\,. \tag{16}$$

We now compute the inner (spatial) quadratures appearing into the last of (16), i.e.

$$
\begin{aligned}
&\jmath k_m \int_0^t \mathrm{d}\tau \int \mathrm{d}\bar{\boldsymbol{x}} \exp\left(-\jmath\, \boldsymbol{k}\cdot\bar{\boldsymbol{x}}\right) G_3\left(|\boldsymbol{x}-\bar{\boldsymbol{x}}|, t-\tau\right) \frac{\partial}{\partial \bar{x}_m} G_2(\bar{x}_r,\tau) = -\frac{\jmath}{2}\exp\left(-\jmath k_3 x_3\right)\times \\
&\int_0^t \frac{\mathrm{d}\tau}{\tau} \exp\left[-k_3^2\left(t-\tau\right)\right] \int \mathrm{d}\bar{\boldsymbol{x}}_r \exp\left(-\jmath\, \boldsymbol{k}_r\cdot\bar{\boldsymbol{x}}_r\right) G_2\left(|\boldsymbol{x}_r-\bar{\boldsymbol{x}}_r|, t-\tau\right) \boldsymbol{k}_r\cdot\bar{\boldsymbol{x}}_r\, G_2(\bar{x}_r,\tau) = \\
&(8\pi)^{-1}\exp\left(-\jmath k_3 x_3\right)\lim_{\alpha\to\jmath}\int_0^t \frac{\mathrm{d}\tau}{\tau^2}\exp\left[-k_3^2\left(t-\tau\right)\right] G_2\left(x_r, t-\tau\right)\alpha\frac{\partial}{\partial\alpha}\mathcal{I}\left(\alpha\right), \qquad (17)
\end{aligned}
$$

where we have set

$$
\mathcal{I}\left(\alpha\right) = \int \mathrm{d}\bar{\boldsymbol{x}}_r \exp\left(-a\bar{x}_r^2\right)\exp\left(\boldsymbol{\omega}_\alpha\cdot\bar{\boldsymbol{x}}_r\right), \qquad (18)
$$

being $\boldsymbol{\omega}_\alpha \equiv b\boldsymbol{x}_r - \alpha\boldsymbol{k}_r$, $a \equiv \dfrac{t}{4\left(t-\tau\right)\tau}$ and $b \equiv \dfrac{1}{2\left(t-\tau\right)}$. The evaluation of $\mathcal{I}\left(\alpha\right)$ is straightforward. By skipping the algebraic details, it yields $\mathcal{I}\left(\alpha\right) = \left(\pi/a\right)\exp\left[\boldsymbol{\omega}_\alpha\cdot\boldsymbol{\omega}_\alpha/\left(4a\right)\right]$. As a consequence, eq. (16) writes as:

$$
G^{(1)}(\boldsymbol{x},t) = -\frac{\jmath}{2t}G_2\left(x_r,t\right)\int\frac{\mathrm{d}\boldsymbol{k}\tilde{Y}\left(\boldsymbol{k}\right)}{\left(2\pi\right)^{3/2}}\exp\left(-\jmath k_3x_3\right)\int_0^t\mathrm{d}\tau\,\Gamma\left(\tau\right)\exp\left[\jmath\frac{t-\tau}{t}\left(\jmath\tau\boldsymbol{k}_r-\boldsymbol{x}_r\right)\cdot\boldsymbol{k}_r\right], \qquad (19)
$$

with $\Gamma\left(t\right) \equiv \left(\boldsymbol{x}_r\cdot\boldsymbol{k}_r - 2\jmath t k_r^2\right)\exp\left(-k_3^2 t\right)$. We are now in position to calculate the fluctuation $h^{(1)}(\boldsymbol{x},t) = \int_0^t \mathrm{d}\tau\, G^{(1)}(\boldsymbol{x},\tau)$ that, after changing the order of integration and performing one quadrature, becomes:

$$
\begin{aligned}
&h^{(1)}(\boldsymbol{x},t) = -\frac{\jmath}{8\pi}\int\frac{\mathrm{d}\boldsymbol{k}\,\tilde{Y}\left(\boldsymbol{k}\right)}{\left(2\pi\right)^{3/2}}\exp\left(-\jmath k_3x_3\right)\exp\left(-\jmath\boldsymbol{x}_r\cdot\boldsymbol{k}_r\right)\int_0^t\mathrm{d}\tau'\,\Gamma\left(\tau'\right)\exp\left(-k_r^2\,\tau'\right)\times \\
&\int_{\tau'}^t\frac{\mathrm{d}\tau''}{\tau''^2}\exp\left(-\frac{\omega_{\tau'}}{4\tau''}\right) = -\frac{\jmath}{2\pi}\int\frac{\mathrm{d}\boldsymbol{k}\,\tilde{Y}\left(\boldsymbol{k}\right)}{\left(2\pi\right)^{3/2}}\exp\left(-\jmath k_3x_3\right)\exp\left(-\jmath\boldsymbol{x}_r\cdot\boldsymbol{k}_r\right)\int_0^t\mathrm{d}\tau\exp\left(-k^2\tau\right) \\
&\times\beta(\tau)\left[\exp\left(-\frac{\omega_\tau}{4u}\right)\right]_{u=\tau}^{u=t}, \quad \omega_t\equiv x_r^2+4\jmath t\left(\jmath t\boldsymbol{k}_r-\boldsymbol{x}_r\right)\cdot\boldsymbol{k}_r, \quad \beta\left(t\right)=\frac{\boldsymbol{k}_r}{\omega_t}\cdot\left(\boldsymbol{x}_r-2\jmath t\boldsymbol{k}_r\right). \qquad (20)
\end{aligned}
$$

As anticipated, we now focus on the large time behavior of (20). Toward this aim, we preliminarily note that, for $t \gg 1$, the dominant contribution in the integrand of (20) (that is achieved upon asymptotic expansion, and by retaining the leading order term) is such that:

$$
\beta\left(\tau\right)\simeq\frac{\jmath}{2\tau}, \qquad \exp\left(-\frac{\omega_\tau}{4t}\right)\simeq\exp\left(-\frac{x_r^2}{4\tau}\right). \qquad (21)
$$

Hence, by replacing the functions $\beta(\tau)$ and $\exp\left[-\omega_\tau/(4t)\right]$ with the approximations (21) leads to:

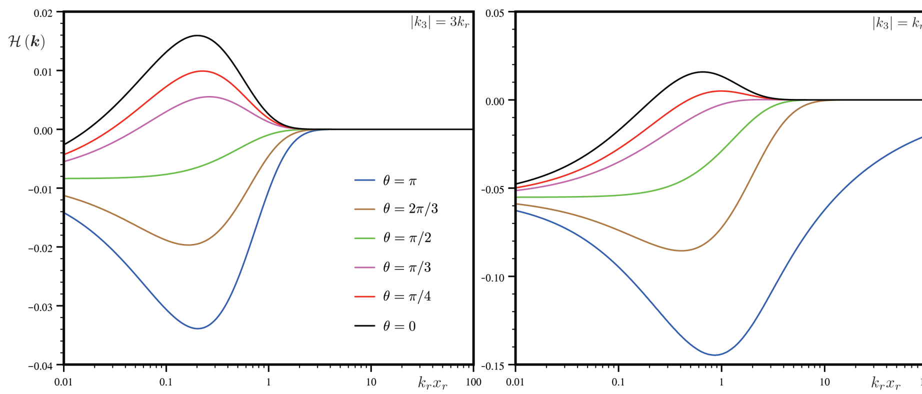

FIG. 2. Dependence of the function $\mathcal{H} \equiv \mathcal{H}(\boldsymbol{k})$ upon the nondimensional distance $k_r\, x_r$ and polar angles $\theta = \arccos\left[\boldsymbol{k}_r \cdot \boldsymbol{x}_r/(k_r\, x_r)\right]$. Other values: $|k_3| = 3k_r$ and $|k_3| = k_r$.

$$h^{(1)}(\boldsymbol{x},t) = -\frac{\jmath}{2\pi}\int \frac{\mathrm{d}\boldsymbol{k}\,\tilde{Y}(\boldsymbol{k})}{(2\pi)^{3/2}}\exp(-\jmath k_3 x_3)\left[\exp(-\jmath \boldsymbol{x}_r\cdot\boldsymbol{k}_r)\int_0^t \mathrm{d}\tau\,\beta(\tau)\,\exp\left(-k^2\tau - \frac{\omega_\tau}{4t}\right)\right.$$
$$\left. - \int_0^t \mathrm{d}\tau\,\beta(\tau)\,\exp\left(-k_3^2\tau - \frac{x_r^2}{4\tau}\right)\right] \simeq \frac{1}{4\pi}\int \frac{\mathrm{d}\boldsymbol{k}\,\tilde{Y}(\boldsymbol{k})}{(2\pi)^{3/2}}\exp(-\jmath k_3 x_3)\left[\exp(-\jmath \boldsymbol{x}_r\cdot\boldsymbol{k}_r)\times\right.$$
$$\left.\int_0^t \frac{\mathrm{d}\tau}{\tau}\exp\left(-k^2\tau - \frac{x_r^2}{4\tau}\right) - \int_0^t \frac{\mathrm{d}\tau}{\tau}\exp\left(-k_3^2\tau - \frac{x_r^2}{4\tau}\right)\right] + \mathcal{O}\left(t^{-1}\right). \tag{22}$$

Finally, by taking the limit $t \to \infty$ in the last of (22) one has:

$$H^{(1)}(\boldsymbol{x}) = \lim_{t\to\infty} h^{(1)}(\boldsymbol{x},t) = \int \frac{\mathrm{d}\boldsymbol{k}\,\tilde{Y}(\boldsymbol{k})}{(2\pi)^{5/2}}\exp(-\jmath k_3 x_3)\left[\exp(-\jmath \boldsymbol{x}_r\cdot\boldsymbol{k}_r)\,\mathrm{K}_0(x_r k) - \mathrm{K}_0(x_r|k_3|)\right], \tag{23}$$

where K_n is the n-order modified Bessel function of the first kind. The comparison of (23) with (12) suggests that:

$$\mathcal{H}(\boldsymbol{k}) = (2\pi)^{-1}\left[\mathrm{K}_0(|\boldsymbol{k}|x_r) - \exp(-\boldsymbol{k}_r\cdot\boldsymbol{x}_r)\,\mathrm{K}_0(|k_3|x_r)\right]. \tag{24}$$

For illustration purposes, the function (24) is depicted in FIG. 2 versus the dimensionless variable $k_r x_r$, a few values of the polar angle $\theta = \arccos\left[\boldsymbol{k}_r\cdot\boldsymbol{x}_r/(k_r\, x_r)\right]$ and two values of $|k_3|$. The quantity $\lim_{x_r\to 0^+}\mathcal{H} = (2\pi)^{-1}\ln(|k_3|/|\boldsymbol{k}|)$ is instrumental in the engineering applications, in order to let the head's fluctuation meet a Dirichlet boundary condition at the source

Accepted to Phys. Fluids 10.1063/5.0147691

(*regularization*). At the other extreme of large distances, the function (24) vanishes with exponential decay. In what follows, we proceed with analyzing second-order moments of the flow variables that, for weakly heterogeneous media, result of the same order of magnitude of the Y- variance $\sigma_Y^2 = \langle Y^2 \rangle$.

DISCUSSION

We wish to derive and discuss some statistical parameters that quantify the uncertainty in the spatial distribution of the specific energy H and the velocity $\boldsymbol{V}$. Starting with the cross-covariance $C_{YH}(\boldsymbol{x},\boldsymbol{y}) \equiv \left\langle Y(\boldsymbol{x})\, H^{(1)}(\boldsymbol{y})\right\rangle$, it results from (23) as:

$$\frac{C_{YH}(\boldsymbol{x},\boldsymbol{y})}{Q\sigma_Y^2} = \int \frac{\mathrm{d}\boldsymbol{k}\,\tilde{\rho}_Y(\boldsymbol{k})}{(2\pi)^{5/2}} \exp(\jmath\xi_3 k_3)\left[\exp(\jmath\boldsymbol{\xi}_r\cdot\boldsymbol{k}_r)\,\mathrm{K}_0(y_r k) - \exp(\jmath\boldsymbol{x}_r\cdot\boldsymbol{k}_r)\,\mathrm{K}_0(y_r|k_3|)\right] \tag{25}$$

($\boldsymbol{\xi} \equiv \boldsymbol{x} - \boldsymbol{y}$), where we have made use of the stationarity of Y, i.e.

$$\left\langle \tilde{Y}(\boldsymbol{k}_1)\,\tilde{Y}(\boldsymbol{k}_2)\right\rangle = (2\pi)^{3/2}\,\sigma_Y^2\,\delta(\boldsymbol{k}_1+\boldsymbol{k}_2)\,\tilde{\rho}_Y(\boldsymbol{k}_2)\,. \tag{26}$$

Likewise, the head covariance $C_H(\boldsymbol{x},\boldsymbol{y}) \equiv \langle H^{(1)}(\boldsymbol{x})H^{(1)}(\boldsymbol{y})\rangle$ is obtained by multiplying (23) applied at two points $\boldsymbol{x} \neq \boldsymbol{y}$, and subsequently taking the ensemble average. The final result is:

$$\begin{aligned}\frac{C_H(\boldsymbol{x},\boldsymbol{y})}{(Q\sigma_Y)^2} = \int \frac{\mathrm{d}\boldsymbol{k}\,\tilde{\rho}_Y(\boldsymbol{k})}{(2\pi)^{7/2}} \exp(\jmath\xi_3 k_3)\big[&\exp(-\jmath\boldsymbol{\xi}_r\cdot\boldsymbol{k}_r)\,\mathrm{K}_0(x_r k)\mathrm{K}_0(y_r k) + \mathrm{K}_0(x_r|k_3|)\mathrm{K}_0(y_r|k_3|) \\ &- \exp(-\jmath\boldsymbol{x}_r\cdot\boldsymbol{k}_r)\,\mathrm{K}_0(x_r k)\mathrm{K}_0(y_r|k_3|) - \exp(\jmath\boldsymbol{y}_r\cdot\boldsymbol{k}_r)\,\mathrm{K}_0(y_r k)\mathrm{K}_0(x_r|k_3|)\big].\end{aligned} \tag{27}$$

It is seen that the covariances (25) and (27) are stationary along the vertical coordinate (i.e. they depend only upon the lag $\xi_3 = x_3 - y_3$), since the mean value $H^{(0)}(x_r) \equiv Q\,G_2^\infty(x_r)$ does not depend upon the elevation. Moreover, based on the existing data-sets (an exhaustive overview can be found in Rubin, 2003), we regard the autocorrelation of Y as axial symmetric, and therefore the spectrum $\tilde{\rho}_Y(\boldsymbol{k}) \equiv \tilde{\rho}_Y(k_r, k_3)$ is an even function of k_r and k_3. Hence, by adopting cylindrical coordinates in wave-number space, i.e. $\boldsymbol{k} \equiv (k_r\cos\theta, k_r\sin\theta, k_3)$, and carrying out the quadrature over the polar angle lead to:

$$\frac{C_{YH}(\boldsymbol{x},\boldsymbol{y})}{Q\sigma_Y^2} = 2\int_0^\infty\!\!\int_0^\infty \frac{\mathrm{d}k_r\mathrm{d}k_3}{(2\pi)^{3/2}}\,k_r\,\tilde{\rho}_Y(k_r,k_3)\cos(\xi_3 k_3)\left[J_0(\xi_r k_r)\mathrm{K}_0(y_r k) - J_0(x_r k_r)\mathrm{K}_0(y_r k_3)\right], \tag{28}$$

Accepted to Phys. Fluids 10.1063/5.0147691

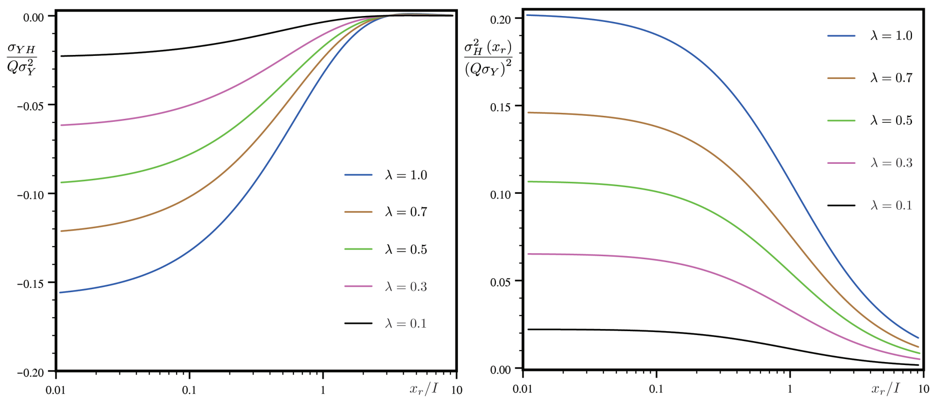

FIG. 3. Dependence of the scaled cross-variance $\sigma_{YH}/(Q\sigma_Y^2)$ and variance $\sigma_H^2/(Q\sigma_Y)^2$ upon the dimensionless distance x_r/I from the source, and several values of the anisotropy ratio λ (exponential spectrum of ρ_Y).

$$\frac{C_H(\boldsymbol{x},\boldsymbol{y})}{(Q\sigma_Y)^2} = 2\int_0^\infty \int_0^\infty \frac{\mathrm{d}k_r \mathrm{d}k_3}{(2\pi)^{5/2}}\, k_r\, \tilde{\rho}_Y\,(k_r,k_3) \cos(\xi_3 k_3) \left[J_0\left(\xi_r k_r\right) \mathrm{K}_0(x_r k)\mathrm{K}_0(y_r k) \right.$$
$$\left. + \mathrm{K}_0(x_r k_3)\mathrm{K}_0(y_r k_3) - J_0\left(x_r k_r\right) \mathrm{K}_0(x_r k)\mathrm{K}_0(y_r k_3) - J_0\left(y_r k_r\right) \mathrm{K}_0(y_r k)\mathrm{K}_0(x_r k_3)\right] \tag{29}$$

(J_n is the n-order Bessel function of the first kind). Two parameters are of particular interest, namely the cross, $\sigma_{YH}\,(x_r) \equiv C_{YH}(\boldsymbol{x},\boldsymbol{x})$, and the head, $\sigma_H^2\,(x_r) \equiv C_H(\boldsymbol{x},\boldsymbol{x})$, variances which are derived from (28)–(29) as follows:

$$\frac{\sigma_{YH}\,(x_r)}{Q\sigma_Y^2} = 2\int_0^\infty \int_0^\infty \frac{\mathrm{d}k_r\, \mathrm{d}k_3}{(2\pi)^{3/2}}\, k_r\, \tilde{\rho}_Y\,(k_r,k_3)\left[\mathrm{K}_0(x_r k) - J_0(x_r k_r)\mathrm{K}_0(x_r k_3)\right], \tag{30}$$

$$\frac{\sigma_H^2(x_r)}{(Q\sigma_Y)^2} = 2\int_0^\infty \int_0^\infty \frac{\mathrm{d}k_r \mathrm{d}k_3}{(2\pi)^{5/2}} k_r \tilde{\rho}_Y\,(k_r,k_3)\left[\mathrm{K}_0^2(x_r k) + \mathrm{K}_0^2(x_r k_3) - 2J_0\left(x_r k_r\right)\mathrm{K}_0(x_r k)\mathrm{K}_0(x_r k_3)\right]. \tag{31}$$

To explore the physical insights of eqs (30)–(31), we adopt an exponential model for the spectrum, i.e. $\tilde{\rho}_Y(k_r,k_3) \equiv (8/\pi)^{1/2}\,\lambda\,(1+k_r^2+\lambda^2 k_3^2)^{-2}$, where the anisotropy ratio $\lambda \in]0,1]$ is defined as the ratio between the vertical, i.e. I_v, and horizontal, i.e. I, integral scales of Y. In addition, the wave numbers $(\boldsymbol{k}_r, k_3)$ have been made dimensionless by replacing $k_i \to I k_i$ (with $\ell_c \equiv I$). In FIG. 3 the cross-variance (30) is depicted as a function of the scaled variable x_r/I and a few values of λ. It is a monotonic increasing function of x_r that

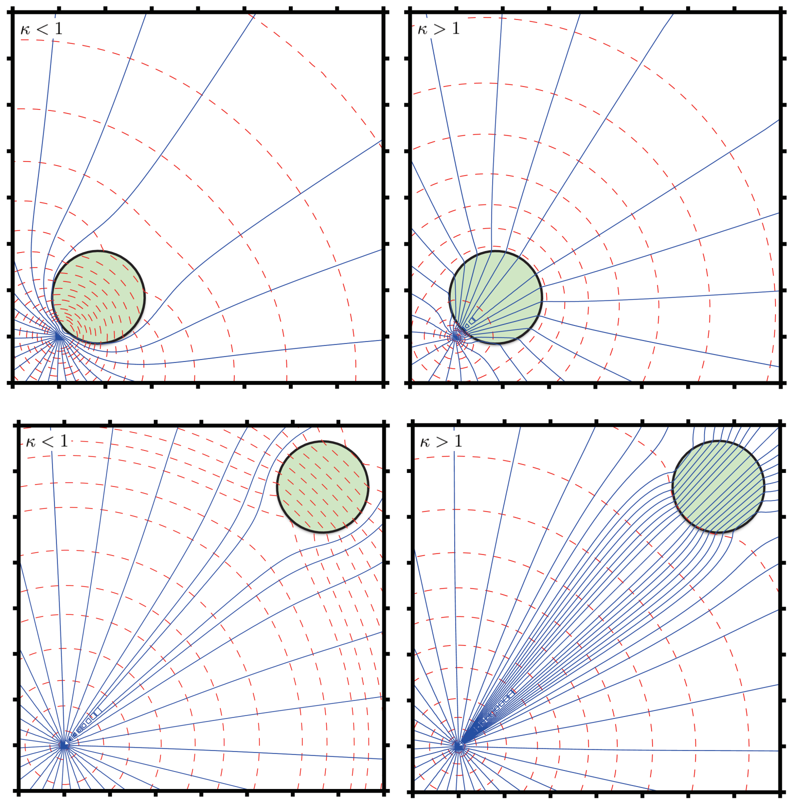

FIG. 4. Contour-plot of the head (red dashed lines) and stream function (blue continuous lines) as affected by a circular (green) inclusion of conductivity K implanted into a matrix of effective conductivity K_{eff}. On the top, pictures refer to an inclusion close to the source with contrast ratio $\kappa = K/K_{\text{eff}}$ smaller and larger than one. Below, pictures pertain to the analogous situation, but for an inclusion lying away from the source.

starts from the value at the source, i.e.

$$\sigma_{YH}(0) = \frac{2Q\sigma_Y^2}{(2\pi)^{3/2}} \int_0^\infty \int_0^\infty \mathrm{d}k_r \mathrm{d}k_3 \, k_r \, \tilde{\rho}_Y(k_r, k_3) \ln \frac{k_3}{k} = -Q\sigma_Y^2 \frac{\lambda}{2\pi} \frac{\arcsin\sqrt{1-\lambda^2}}{\sqrt{1-\lambda^2}}, \quad (32)$$

and it vanishes after four horizontal integral scales. In particular, the near field (32) is valid also for a Gaussian spectrum: $\tilde{\rho}_Y(k_r, k_3) \equiv (2/\pi)^{3/2} \lambda \exp(-k_r^2/\pi - \lambda^2 k_3^2/\pi)$.

In order to explain the behavior of the cross-variance σ_{YH}, we can focus on the flow's pattern as deformed by a single inclusion of conductivity K (Severino, 2019) embedded into a matrix of effective conductivity K_{eff} (being σ_{YH} evaluated as average of the product between the fluctuations $H^{(1)}$ and Y over many of such realizations). Thus, in the FIG. 4 we have depicted a circular (green) inclusion near and far from the source for two largely different values of the *contrast ratio* $\kappa \equiv K/K_{\text{eff}}$. In particular, due to the mass conservation, the streamlines circumvent the inclusion for $\kappa < 1$ and they are attracted by it for $\kappa > 1$. As a consequence, in the near and far field the head surrounding the inclusion results higher/lower than the mean head (corresponding to $\kappa = 1$) for $\kappa < 1$ and $\kappa > 1$, respectively. Thus, for $\kappa < 1$ (calling for $Y < 0$) the fluctuation $H^{(1)}$ is larger than the mean, and *viceversa*. Hence, the product $Y(x_r)\, H^{(1)}(x_r)$ (and concurrently the ensemble average σ_{YH}) results lesser than zero, in any case. The limit $\lim\limits_{x_r\to\infty} \sigma_{YH}(x_r) = 0$ is explained by recalling that the head's fluctuation tends to zero away from the source (see (23)). Finally, the reduction of σ_{YH} (for given x_r) with increasing λ has a straightforward kinematical reasoning: an anisotropic medium can be sought as made up by inclusions elongated in the horizontal direction (resembling the medium's structure $\lambda \equiv I_v/I < 1$). Thus, for a fluid particle it is easier to circumvent a low conducting inclusion by moving vertically rather than laterally. This causes a deviation from the mean lesser than that which one would observe within a medium of isotropic ($\lambda = 1$) heterogeneity's structure.

By the same token, one can analyze the scaled variance $\sigma_H^2/(Q\sigma_Y)^2$. Thus, at large x_r the head is quite small, since the flow there behaves as a homogeneous one (Abramovich and Indelman, 1995), which decays like x_r^{-1}. To the contrary, in the region close to the source the mean head $H^{(0)}$ is highly uncertain, since most of the head buildup takes place within a tiny annulus surrounding the source (Severino, Leveque, and Toraldo, 2019). The dependence of σ_H^2 upon the anisotropy ratio λ (at any given distance) is explained by the same argument as before.

The variance $\sigma_u^2(x_r) \equiv u_{rr}(x_r, x_r)$ of the velocity is obtained from (9) as:

$$\sigma_u^2(x_r) = \sigma_Y^2\, U^2(x_r) + 2\,\frac{K_G}{n}\, U(x_r)\,\sigma_{YE_r}(x_r) + \left(\frac{K_G}{n}\right)^2 \sigma_{E_r}^2(x_r), \quad E_r \equiv \frac{\partial}{\partial x_r} H^{(1)}(\boldsymbol{x}), \tag{33}$$

where we have set $\sigma_{YE_r} \equiv \langle Y E_r\rangle$ and $\sigma_{E_r}^2 \equiv \langle E_r^2\rangle$. By differentiation of (23), the latter are given by:

$$\sigma_{YE_r}(x_r) = \frac{2Q\sigma_Y^2}{(2\pi)^{3/2}} \int_0^\infty \int_0^\infty \mathrm{d}k_r\, \mathrm{d}k_3\, k_r\, \tilde{\rho}_Y(k_r, k_3)\left[k_3 J_0(x_r k_r)\mathrm{K}_1(x_r k_3) - k\mathrm{K}_1(x_r k)\right], \tag{34}$$

$$\sigma^2_{E_r}(x_r) = \frac{(Q\sigma_Y)^2}{(2\pi)^{5/2}} \int_0^\infty \int_0^\infty \mathrm{d}k_r\, \mathrm{d}k_3\, k_r\, \tilde{\rho}_Y(k_r, k_3) \left\{ 2\left[k \mathrm{K}_1(x_r k)\right]^2 + 2\left[k_3 \mathrm{K}_1(x_r k_3)\right]^2 - \left[k_r \mathrm{K}_0(x_r k)\right]^2 - 2k_3 \mathrm{K}_1(x_r k_3)\left[k_r J_1(x_r k_r) + 2k J_0(x_r k_r) \mathrm{K}_1(x_r k) + k_r J_1(x_r k_r) \mathrm{K}_0(x_r k)\right] \right\}. \tag{35}$$

The scaled coefficient of variation $\mathtt{CV}_u/\sigma_Y = \sigma_u/(U\sigma_Y)$ is depicted (for both exponential and Gaussian $\tilde{\rho}_Y$) in the FIG. 5. It is seen that in the near (i.e. $x_r \ll I$) and far (i.e. $x_r \gg I$) field, one has $\sigma_u \sim \sigma_Y U$. Indeed, close to the source the flow can be homogenized by the harmonic (constant) conductivity (Indelman, 1996), whereas far from the source it behaves like a mean uniform one of effective conductivity. As a consequence, in these two regimes the uncertainty in the velocity field resembles precisely the reduction of the mean velocity U with the distance. In the intermediate regime, for $x_r < I$ the cross-variance (that is negative) is mostly influential, and concurrently $\mathtt{CV}_u$ reduces, whereas for $x_r > I$ it rapidly exhausts, with a still impact of the head-gradient's variance $\sigma^2_{E_r}$. This justifies the sudden rise of $\mathtt{CV}_u$. As it will be clearer later on, these findings are of paramount importance when analyzing the evolution of scattering. To conclude this section, we note that the Gaussian shape of ρ_Y produces a more persistent signal in the coefficient of variation of the velocity (in agreement with Severino and Cuomo, 2020).

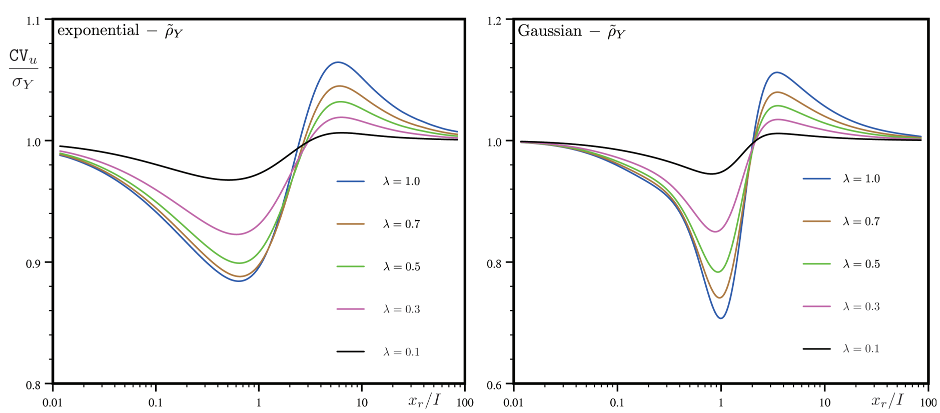

FIG. 5. Scaled coefficient of variation $\mathtt{CV}_u/\sigma_Y$ versus the normalized distance x_r/I from the source, and a few values of the anisotropy ratio λ (exponential and Gaussian spectrum).

SCATTERING ANALYSIS

We are now in position to analyze scattering of a passive scalar as determined by the above discussed source-type flow. This goal is achieved by means of the second-order radial moment (8) which, for convenience of discussion, is re-written on the base of (9) as:

$$X_{rr}(R) = \mathcal{X}_\infty(R) + \mathcal{X}_\star(R)\,, \tag{36}$$

being

$$\mathcal{X}_\infty(R) = \sigma_Y^2\, U^2(R) \int_0^R \int_0^R \mathrm{d}x_r'\, \mathrm{d}x_r''\, \frac{\rho_Y(x_r' - x_r'')}{U(x_r')\, U(x_r'')} = \frac{\sigma_Y^2}{3}\, R \int_0^R \mathrm{d}u \left(2 - 3\frac{u}{R} + \frac{u^3}{R^3}\right) \rho_Y(u)\,, \tag{37}$$

whereas

$$\begin{aligned}\mathcal{X}_\star(R) = {} & U^2(R) \int_0^R \int_0^R \frac{\mathrm{d}x_r'\, \mathrm{d}x_r''}{U^2(x_r')\, U^2(x_r'')} \left[\left(\frac{K_G}{n}\right)^2 \frac{\partial^2}{\partial x_r' \partial x_r''} \left\langle H^{(1)}(x_r')\, H^{(1)}(x_r'')\right\rangle - \right. \\ & \left. \frac{K_G}{n}\, U(x_r') \frac{\partial}{\partial x_r''} \left\langle Y(x_r')\, H^{(1)}(x_r'')\right\rangle - \frac{K_G}{n}\, U(x_r'') \frac{\partial}{\partial x_r'} \left\langle H^{(1)}(x_r')\, Y(x_r'')\right\rangle \right] = \frac{K_G}{n}\, U^2(R) \times \\ & \int_0^R \int_0^R \frac{\mathrm{d}x_r'\, \mathrm{d}x_r''}{U^2(x_r')\, U^2(x_r'')} \left[\left(\frac{K_G}{n}\right) \frac{\partial^2 C_H(x_r', x_r'')}{\partial x_r' \partial x_r''} - 2\, U(x_r') \frac{\partial\, C_{YH}(x_r', x_r'')}{\partial x_r''}\right].\end{aligned} \tag{38}$$

In particular, the last of (38) has been achieved by noting that (x_r', x_r'') is a pair of dummy variables. Then, insertion into (38) of (28)–(29) (with $\xi_3 = 0$) yields:

$$\frac{X_{rr}(R)}{\sigma_Y^2} = \frac{R}{3} \int_0^R \mathrm{d}u \left(2 - 3\frac{u}{R} + \frac{u^3}{R^3}\right) \rho_Y(u) + \frac{\sqrt{2/\pi}}{R^2}\, \bar{\mathcal{X}}_\star(R)\,, \tag{39}$$

where we have set:

$$\bar{\mathcal{X}}_\star = \int_0^\infty \int_0^\infty \int_0^R \int_0^R \mathrm{d}k_r\, \mathrm{d}k_3\, \mathrm{d}x\, \mathrm{d}y\, k_r\, \tilde{\rho}_Y(k_r, k_3)\, y^2 \frac{\partial}{\partial y} \left[x^2 \frac{\partial}{\partial x} \Psi_H(x, y) - x\, \Psi_{YH}(x, y)\right], \tag{40}$$

$$\Psi_{YH}(x, y) = J_0(k_r\,|x - y|)\, \mathrm{K}_0(ky) - J_0(k_r x)\, \mathrm{K}_0(k_3 y), \quad k = \sqrt{k_r^2 + k_3^2}\,, \tag{41}$$

$$\Psi_H(x, y) = \mathrm{K}_0(kx)\, \Psi_{YH}(x, y) + \mathrm{K}_0(k_3 x)\left[\mathrm{K}_0(k_3 y) - J_0(k_r y)\, \mathrm{K}_0(ky)\right]. \tag{42}$$

Hence, integration by parts in the domain $[0, R] \times [0, R]$ enables one to decompose the integral (40) as $\bar{\mathcal{X}}_\star = 4\mathcal{X}_4 - 2R^2\mathcal{X}_3 + R^4\mathcal{X}_2$, with

$$\mathcal{X}_2(R) = \int_0^\infty \int_0^\infty \mathrm{d}k_r\, \mathrm{d}k_3\, k_r\, \tilde{\rho}_Y(k_r, k_3)\, \Psi_H(R, R)\,, \tag{43}$$

Accepted to Phys. Fluids 10.1063/5.0147691

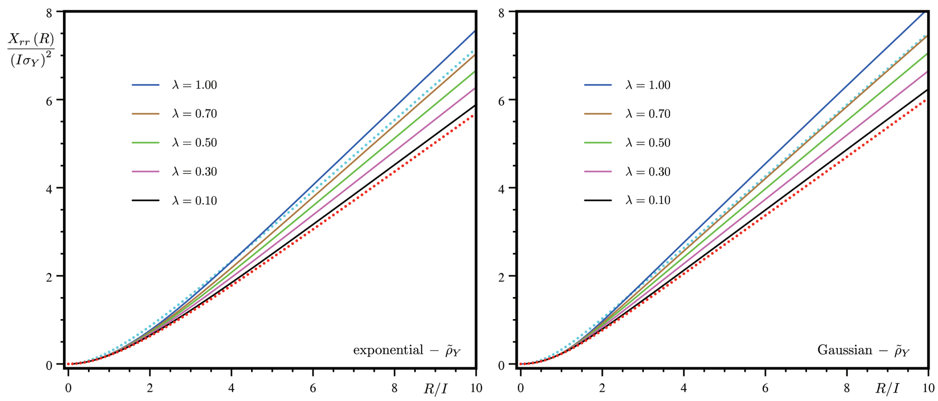

FIG. 6. Scaled trajectory variance $X_{rr}/(I\sigma_Y)^2$ as computed from (39) for several values of the anisotropy ratio λ (exponential and Gaussian spectrum $\tilde{\rho}_Y$). Dot red and cyan lines refer to eqs (46) and (47), respectively.

$$\mathcal{X}_3(R) = \int_0^\infty \int_0^\infty \int_0^R \mathrm{d}k_r\, \mathrm{d}k_3\, \mathrm{d}x\, k_r\, \tilde{\rho}_Y(k_r, k_3)\, x \left[\Psi_H(x,R) + \frac{1}{2}\Psi_{YH}(x,R) + \Psi_H(R,x)\right], \tag{44}$$

$$\mathcal{X}_4(R) = \int_0^\infty \int_0^\infty \int_0^R \int_0^R \mathrm{d}k_r\, \mathrm{d}k_3\, \mathrm{d}x\, \mathrm{d}y\, k_r\, \tilde{\rho}_Y(k_r, k_3)\, x\, y \left[\Psi_H(x,y) + \frac{1}{2}\Psi_{YH}(x,y)\right]. \tag{45}$$

The utility related to the decomposition in (36), and the subsequent developments, relies on the fact that one can clearly distinguish the contribution (i.e. $\mathcal{X}_\infty$) due to the mean radial flow from that (i.e. $\mathcal{X}_\star$) associated to the fluctuation of the head-gradient. In the FIG. 6 we have depicted the scaled moment $X_{rr}/(I\sigma_Y)^2$ versus the non dimensional travel distance R/I, and $\lambda = 0.1; 0.3; 0.5; 0.7; 1.0$. It has been done for both exponential and Gaussian spectrum. For comparison purposes, we have also depicted (red dot line) the approximation $X_{rr} \simeq \mathcal{X}_\infty$:

$$X_{rr}(R) \simeq \frac{(I\sigma_Y)^2}{3\pi^2 R^2} \begin{cases} \pi^2\left[2R^3 - 3R^2 + 6 - 6(R+1)\exp(-R)\right] & \text{(exp)} \\ 8 - 6\pi R^2 + 2\pi^2 R^3 \operatorname{erf}\left(\frac{\sqrt{\pi}}{2}R\right) + 4\left(\pi R^2 - 2\right)\exp\left(-\frac{\pi}{4}R^2\right) & \text{(Gauss)} \end{cases} \tag{46}$$

which is valid for $\lambda \ll 1$ (Indelman and Dagan, 1999), along with a newly derived approximate (cyan dot line) expression of X_{rr}, i.e.

$$X_{rr} \simeq \frac{(I\sigma_Y)^2}{27\pi^2 R^2} \begin{cases} \pi^2 \left[22R^3 - 27R^2 + 30 + 6\left(2R^2 - 5R - 5\right)\exp\left(-R\right)\right] & \text{(exp)} \\ 40 - 54\pi R^2 + 22\pi^2 R^3 \mathrm{erf}\left(\frac{\sqrt{\pi}}{2}R\right) + 4\left(11\pi R^2 - 10\right)\exp\left(-\frac{\pi}{4}R^2\right) & \text{(Gauss)} \end{cases} \tag{47}$$

(for details, see the APPENDIX).

As particles are injected through the source in the porous medium, the radial moment X_{rr} increases monotonically with R. At short distances, X_{rr} displays a nonlinear dependence, whereas at large distances it grows linearly. These findings rely upon the dependence of X_{rr} on the velocity covariance through eq. (8) that, in turn, is a measure of the distance over which the velocities of two fluid particles are correlated. As a consequence, for $R \ll I$ two fluid particles have not covered a single integral scale I, and concurrently they are highly correlated. As a consequence, scattering results enhanced by the dominant impact of the velocity covariance u_{rr}. Conversely, at large distances the advective velocity drops like x_r^{-1}, and the net, overall effect is still an increasing scattering, but with a lesser gradient. In order to address such a behavior in a quantitative manner, one can refer either to the approximate expression of Indelman and Dagan (1999), i.e. $X_{rr}(R) \simeq (\sigma_Y^2 R/3)\int_0^R \mathrm{d}u\,(2 - 3u/R + u^3/R^3)\,\rho_Y(u)$, or to eq. (A13), i.e. $X_{rr}(R) \simeq (\sigma_Y^2 R/27)\int_0^R \mathrm{d}u\,(22 - 27u/R + 5u^3/R^3)\,\rho_Y(u)$. Thus, at small distances it yields $\rho_Y \sim 1$, and one recovers that $X_{rr} \sim R^2$. Instead, at large R one has $u/R = \mathrm{o}(1)$, and therefore $X_{rr} \sim R\int_0^\infty \mathrm{d}u\,\rho_Y(u) = R$. The reduction of X_{rr} with the small λ-values is explained similarly to the above discussion: for a solute particles it is easier to circumvent, by taking a vertical step, a poorly conducting inclusion characterized by $\lambda \ll 1$ as compared with an inclusion of quasi isotropic (i.e. $\lambda \simeq 1$) heterogeneity's structure. As a consequence, the deviation from the mean is larger in the latter case, and this explains the increasing (for given R) trajectory's variance as $\lambda \to 1$. Finally, besides the clear agreement (see FIG. 6) in the case of strongly heterogeneous formation ($\lambda \ll 1$), the complete expression (39) of the radial second-order moment was found in perfect overlapping with the numerical simulations shown in the FIG. 4 of Indelman and Dagan (1999). Moreover, inspection from FIG. 6 suggests that the approximate expression (47) is found in a reasonable agreement with the full simulation of X_{rr} in the regime of pseudo-isotropic ($\lambda \lesssim 1$) formations. To conclude, equations (46)–(47) are straightforwardly extended to disordered media of axial symmetric heterogeneity's structure by replacing $R \to R/\sqrt{\cos^2\phi + \lambda^{-2}\sin^2\phi}$, being ϕ the angle between the mean trajectory and the plane of isotropy.

CONCLUDING REMARKS

Scattering processes generated by localized/distributed sources are a powerful tool which finds application in numerous branches of applied sciences. In quantum physics, scattering is used to infer the size as well as the distribution of the electrical charge of nuclei, whereas in the electrodynamics it serves to compute dielectric properties. In the theory of composites and in the reservoir engineering (the fields of main concern for the present study), it serves to identify the effective (flow and transport) properties of disordered media.

We have focused on scattering of a passive scalar injected in a formation and advected by a steady velocity, that in turn is generated by a line of singularity. Within a homogeneous domain, the solute propagates by advection like a cylinder of radius $R \equiv R(t)$, whereas scattering is due to the diffusion mechanism, solely (FIG. 1). In disordered media, scattering is determined by the fluctuations of the advective velocity which are caused by the erratic, spatial variability of the conductivity K. Within a stochastic framework, that regards the log-conductivity $\ln K$ as a stationary, Gaussian, random field, scattering is quantified by means of the second-order radial moment which, by virtue of ergodicity, coincides with the trajectory variance (8). After adopting a few simplifying assumptions (the most relevant of which requires that the variance of $\ln K$ is much smaller than one), it is shown that, central for the study, is the computation of the integral (12). Despite its origin, it is recognized that such a quantity is instrumental for many other problems arising in several branches of classical as well as quantum physics, and therefore its study results of a much wider interest than that strictly considered here. The analytical computation of (12) is achieved as large time limit of the same problem in the unsteady state flow regime.

Unlike past studies on the same topic (see, e.g. Fiori, Indelman, and Dagan, 1998), here covariances of the flow variables are expressed in terms of two quadratures solely, which are easily carried out after specifying the shape of the spectrum (the Fourier transform of the autocorrelation of Y). Illustrations focus on the (cross)-variances of the specific energy and the radial velocity, since they are usually of interest in the applications. It is seen that, although the log-conductivity is a stationary random field, these variances are not since the mean flow is not uniform.

The trajectory variance X_{rr} is computed and discussed for both exponential and Gaussian spectrum, being these models generally adopted in the real world applications (Dagan, 1989). In particular, the transitional regime from the early to the large distances is much more persistent than that pertaining to the approximation valid for formations with an anisotropic ratio λ much lesser than one (Indelman and Dagan, 1999). This approximation does not lend itself to investigate scattering when the formation is (pseudo)isotropic ($\lambda \lesssim 1$). In these cases, our results fill the gap (and, more generally, they cover the entire range $\lambda \in [0, 1]$). Finally, another point of novelty of the present study is that, similarly to Indelman and Dagan (1999), we have obtained an approximate, simple (closed form) solution (A13) that applies in the regime of (pseudo)isotropic heterogeneity.

To conclude, results achieved in the present study can be expanded along (at least) two avenues: i) by computing higher-order corrections to the various terms appearing into the velocity covariance u_{rr} (similarly to Abramovich and Indelman, 1995), or ii) by reformulating the entire problem in the context of the self-consistent approximation (in close analogy to Dagan, Fiori, and Janković, 2003).

ACKNOWLEDGMENTS

The present study was developed within the GNCS (*Gruppo Nazionale Calcolo Scientifico* - INdAM) framework, and it was supported by the project # 3778/2022 (Departmental fund). The final release of all the figures was achieved thanks to the computer artistry of Dr Gugliemo BRUNETTI, to whom we are greatly indebted. We thank the anonymous Referees for their comments, which have significantly improved the early version of the manuscript.

DATA AVAILABILITY AND AUTHOR DECLARATIONS

The data that support the findings of this study are available from the corresponding author (gerardo.severino@unina.it) upon reasonable request. The Authors have no conflicts to disclose.

APPENDIX: derivation of the approximate expression (47)

As a preparatory step, we re-write the last of (38) as:

$$\mathcal{X}_\star(R)=\left(\frac{2\pi}{QR}\right)^2\int_0^R\int_0^R \mathrm{d}x_r'\,\mathrm{d}x_r''\,(x_r'\,x_r'')^2\,\frac{\partial}{\partial x_r''}\left[\frac{\partial}{\partial x_r'}\,C_H(x_r',x_r'')-\frac{Q}{\pi x_r'}\,C_{YH}(x_r',x_r'')\right]=$$
$$\left(\frac{2\pi}{QR}\right)^2\int_0^R\int_0^R \mathrm{d}x_r'\,\mathrm{d}x_r''\,(x_r'\,x_r'')^2\,\frac{\partial}{\partial x_r''}\left[\frac{\partial\,C_H(x_r',x_r'')}{\partial x_r'}+2\,C_{YH}(x_r',x_r'')\,\frac{\partial\,H^{(0)}(x_r')}{\partial x_r'}\right].\quad\text{(A1)}$$

Then, the last double integral in (A1) is re-written as:

$$\int_0^R \mathrm{d}x_r''\,x_r''^2\,\frac{\partial}{\partial x_r''}\int_0^R \mathrm{d}x_r'\,x_r'^2\left[\frac{\partial\,C_H(x_r',x_r'')}{\partial x_r'}+2\,C_{YH}(x_r',x_r'')\,\frac{\partial\,H^{(0)}(x_r')}{\partial x_r'}\right]\simeq$$
$$-\frac{1}{3}\int_0^R\int_0^R \mathrm{d}x_r'\,\mathrm{d}x_r''\,x_r'^3x_r''^2\,\frac{\partial}{\partial x_r''}\left[\frac{\partial^2\,C_H(x_r',x_r'')}{\partial x_r'^2}+2\frac{\partial\,H^{(0)}(x_r')}{\partial x_r'}\frac{\partial\,C_{YH}(x_r',x_r'')}{\partial x_r'}\right],\qquad\text{(A2)}$$

where the second passage in (A2) has been achieved upon integration by parts and neglecting the finite term due to its very fast (exponential) decay with R. In addition, the term $2x_r'^3C_{YH}(x_r',x_r'')\,\frac{\partial^2}{\partial x_r^2}H^{(0)}(x_r)$ (that also arises upon application of integration by parts) has been dropped out, since, from the definition of two-dimensional Green function, one has $\frac{\partial^2}{\partial x_r^2}H^{(0)}(x_r)=-Q\delta(\boldsymbol{x}_r)$.

At this stage, we note that the governing equation (5) for the head's fluctuation can be written in approximate manner as follows:

$$-\left(\nabla_r^2+\frac{\partial^2}{\partial x_3^2}\right)H^{(1)}(\boldsymbol{x})\simeq-\nabla_r^2H^{(1)}(\boldsymbol{x})=\nabla_r\,H^{(0)}(x_r)\cdot\nabla_rY(\boldsymbol{x}).\qquad\text{(A3)}$$

The neglect of the second-order derivative $\frac{\partial^2}{\partial x_3^2}$ as compared with the laplacian ∇_r^2 is authorized by the fact that most of the flow develops radially, and therefore the dominant variations of the head's fluctuation occur in the horizontal plane. In order to provide a quantitative reasoning, we recall that $\frac{\partial^2}{\partial x_3^2}\sim\mathcal{O}(I_v^{-2})$, whereas $\nabla_r^2\sim\mathcal{O}(I^{-2})$. As a consequence, the ratio of the two estimates behaves like $(I_v/I)^2=\lambda^2$. Since, the majority of the natural formations are anisotropic ($\lambda\leq 1$), we argue that the above approximation works quite well (see also discussion in Indelman and Dagan, 1999). Hence, upon multiplication of (A3) by the head's fluctuation evaluated at $\boldsymbol{y}_r\neq\boldsymbol{x}_r$, and taking the ensemble average, it leads to:

$$-\nabla_r^2\,C_H(x_r,y_r)=\nabla_r\,H^{(0)}(x_r)\cdot\nabla_r\,C_{YH}(x_r,y_r).\qquad\text{(A4)}$$

Then, application of the chain rule of derivation $\frac{\partial}{\partial x_m} \equiv \frac{x_m}{x_r}\frac{\partial}{\partial x_r}$ $(m = 1, 2)$ enables one to write (A4) as:

$$\frac{\partial^2}{\partial x_r^2} C_H(x_r, y_r) = -\frac{\partial}{\partial x_r} H^{(0)}(x_r) \frac{\partial}{\partial x_r} C_{YH}(x_r, y_r), \tag{A5}$$

and the subsequent substitution into the last of (A2) permits to write $\mathcal{X}_\star$ as:

$$\mathcal{X}_\star(R) = -\frac{1}{3}\left(\frac{2\pi}{QR}\right)^2 \int_0^R \int_0^R \mathrm{d}x'_r\, \mathrm{d}x''_r\, x_r'^3 x_r''^2 \frac{\partial H^{(0)}(x'_r)}{\partial x'_r} \frac{\partial^2 C_{YH}(x'_r, x''_r)}{\partial x'_r \partial x''_r}. \tag{A6}$$

By taking integration by parts in (A6) with respect to the variable x''_r, it yields (with the same reasoning as before):

$$\mathcal{X}_\star(R) = \left(\frac{2\pi}{3QR}\right)^2 \int_0^R \int_0^R \mathrm{d}x'_r\, \mathrm{d}x''_r\, (x'_r x''_r)^3 \frac{\partial H^{(0)}(x'_r)}{\partial x'_r} \frac{\partial}{\partial x'_r}\left[\frac{\partial^2 C_{YH}(x'_r, x''_r)}{\partial x_r''^2}\right]. \tag{A7}$$

Likewise, one can write:

$$\frac{\partial^2}{\partial y_r^2} C_{YH}(x_r, y_r) = -\sigma_Y^2 \frac{\partial}{\partial y_r} H^{(0)}(y_r) \frac{\partial}{\partial y_r} \rho_Y(x_r - y_r), \tag{A8}$$

and therefore eq. (A7) reads as:

$$\mathcal{X}_\star(R) = -\left(\frac{2\pi\sigma_Y}{3QR}\right)^2 \int_0^R \int_0^R \mathrm{d}x'_r\, \mathrm{d}x''_r\, (x'_r x''_r)^3 \frac{\partial H^{(0)}(x'_r)}{\partial x'_r} \frac{\partial^2 \rho_Y(x'_r - x''_r)}{\partial x'_r \partial x''_r} \frac{\partial H^{(0)}(x''_r)}{\partial x''_r}. \tag{A9}$$

By noting that:

$$\frac{\partial}{\partial x_r} H^{(0)}(x_r) = -\frac{Q}{2\pi x_r}, \qquad \frac{\partial^2}{\partial x_r \partial y_r} \rho_Y(x_r - y_r) \equiv -\frac{\mathrm{d}^2}{\mathrm{d}u^2} \rho_Y(u)\Big|_{u = x_r - y_r}, \tag{A10}$$

eq. (A9) becomes:

$$\mathcal{X}_\star(R) = \left(\frac{\sigma_Y}{3R}\right)^2 \int_0^R \int_0^R \mathrm{d}x'_r\, \mathrm{d}x''_r\, (x'_r x''_r)^2 \frac{\mathrm{d}^2}{\mathrm{d}u^2} \rho_Y(u)\Big|_{u = x'_r - x''_r}. \tag{A11}$$

Hence, the computation of one quadrature leads to:

$$\mathcal{X}_\star(R) = \frac{\sigma_Y^2}{135} R^3 \int_0^R \mathrm{d}u \left(6 - 15\frac{u}{R} + 10\frac{u^2}{R^2} - \frac{u^5}{R^5}\right) \frac{\mathrm{d}^2}{\mathrm{d}u^2} \rho_Y(u), \tag{A12}$$

and the application (two times) of integration by parts provides (on the same grounds of the above adopted approximation) the final result:

$$X_{rr}(R) = \mathcal{X}_\infty(R) + \mathcal{X}_\star(R) \simeq \frac{\sigma_Y^2}{27} R \int_0^R \mathrm{d}u \left(22 - 27\frac{u}{R} + 5\frac{u^3}{R^3}\right) \rho_Y(u). \tag{A13}$$

Finally, insertion into (A13) of exponential and Gaussian autocorrelation ρ_Y leads to (47).

REFERENCES

Abramovich, B. and Indelman, P., "Effective permittivity of log-normal isotropic random media," Journal of Physics A: Mathematical and General **28**, 693–700 (1995).

Chin, D. A., "An assessment of first-order stochastic dispersion theories in porous media," Journal of hydrology **199**, 53–73 (1997).

Dagan, G., *Flow and Transport in Porous Formation* (Springer-Verlag, New York, 1989).

Dagan, G., Fiori, A., and Janković, I., "Flow and transport in highly heterogeneous formations: 1. conceptual framework and validity of first-order approximations," Water Resources Research **39** (2003), 10.1029/2002WR001717.

Fiori, A., Indelman, P., and Dagan, G., "Correlation structure of flow variables for steady flow toward a well with application to highly anisotropic heterogeneous formations," Water Resources Research **34**, 699–708 (1998).

Indelman, P., "Averaging of unsteady flows in heterogeneous media of stationary conductivity," Journal of Fluid Mechanics **310**, 39–60 (1996).

Indelman, P. and Dagan, G., "Solute transport in divergent radial flow through heterogeneous porous media," Journal of Fluid Mechanics **384**, 159–182 (1999).

Indelman, P. and Rubin, Y., "Solute transport in nonstationary velocity fields," Water resources research **32**, 1259–1267 (1996).

Jackson, J. D., *Classical electrodynamics* (John Wiley & Sons, New York, 2007).

Koplik, J., Redner, S., and Hinch, E., "Tracer dispersion in planar multipole flows," Physical Review E **50**, 4650 (1994).

Kurowski, P., Ippolito, I., Hulin, J., Koplik, J., and Hinch, E., "Anomalous dispersion in a dipole flow geometry," Physics of Fluids **6**, 108–117 (1994).

Le Borgne, T., Dentz, M., and Carrera, J., "Lagrangian statistical model for transport in highly heterogeneous velocity fields," Phys. Rev. Lett. **101**, 090601 (2008).

Martin, B. R. and Shaw, G., *Nuclear and particle physics: an introduction* (John Wiley & Sons, 2019).

Milton, G. W., *The theory of composites* (Cambridge University Press, 2002).

Rubin, Y., *Applied Stochastic Hydrogeology* (Oxford University Press, Oxford, 2003).

Severino, G., "Macrodispersion by point-like source flows in randomly heterogeneous porous media," Transport in Porous Media **89**, 121–134 (2011).

Severino, G., "Effective conductivity in steady well-type flows through porous formations," Stochastic Environmental Research and Risk Assessment **33(3)**, 827–835 (2019).

Severino, G. and Cuomo, S., "Uncertainty quantification of unsteady flows generated by line-sources through heterogeneous geological formations," SIAM/ASA Journal on Uncertainty Quantification **8**, 807–825 (2020).

Severino, G., Leveque, S., and Toraldo, G., "Uncertainty quantification of unsteady source flows in heterogeneous porous media," Journal of Fluid Mechanics **10**, 5–26 (2019).

Tarek, A., *Reservoir engineering handbook* (Gulf professional publishing, 2018).

Tartakovsky, A. M., Tartakovsky, D. M., and Meakin, P., "Stochastic Langevin model for flow and transport in porous media," Phys. Rev. Lett. **101**, 044502 (2008).

Accepted to Phys. Fluids 10.1063/5.0147691

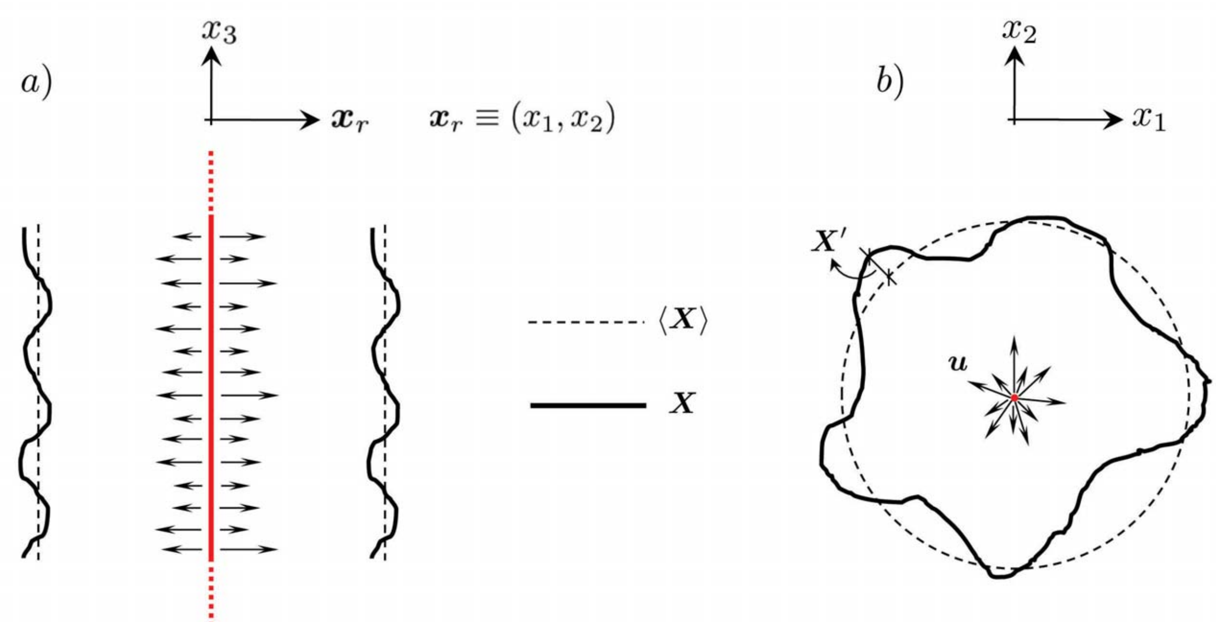

Accepted to Phys. Fluids 10.1063/5.0147691

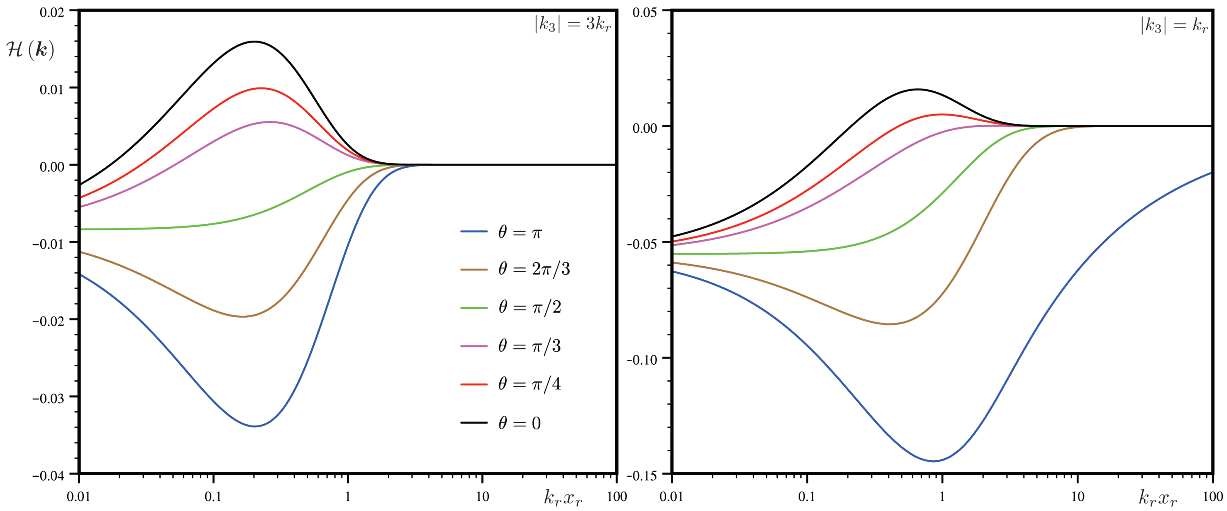

Accepted to Phys. Fluids 10.1063/5.0147691

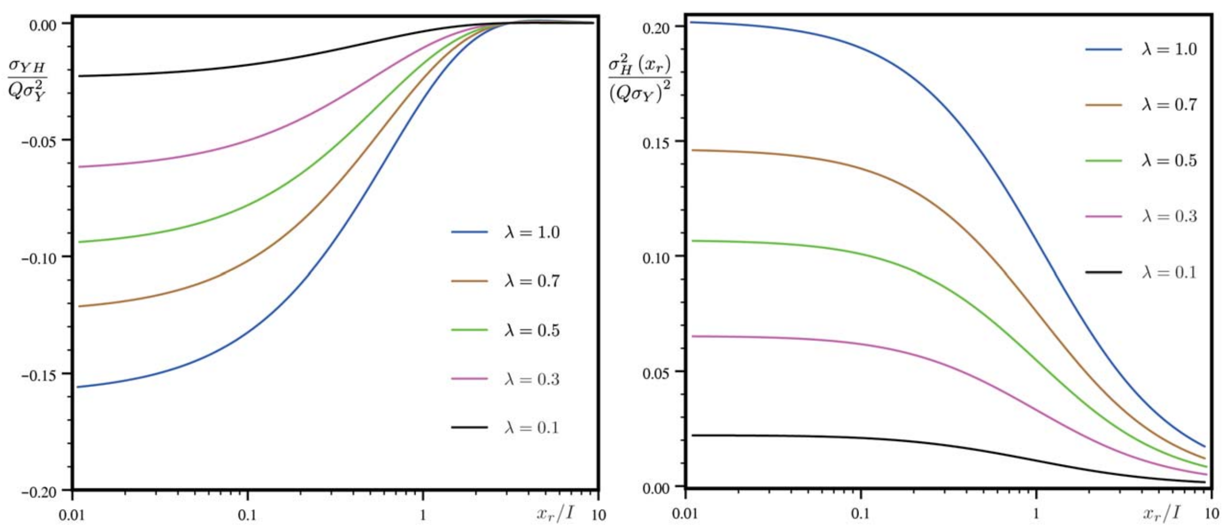

Accepted to Phys. Fluids 10.1063/5.0147691

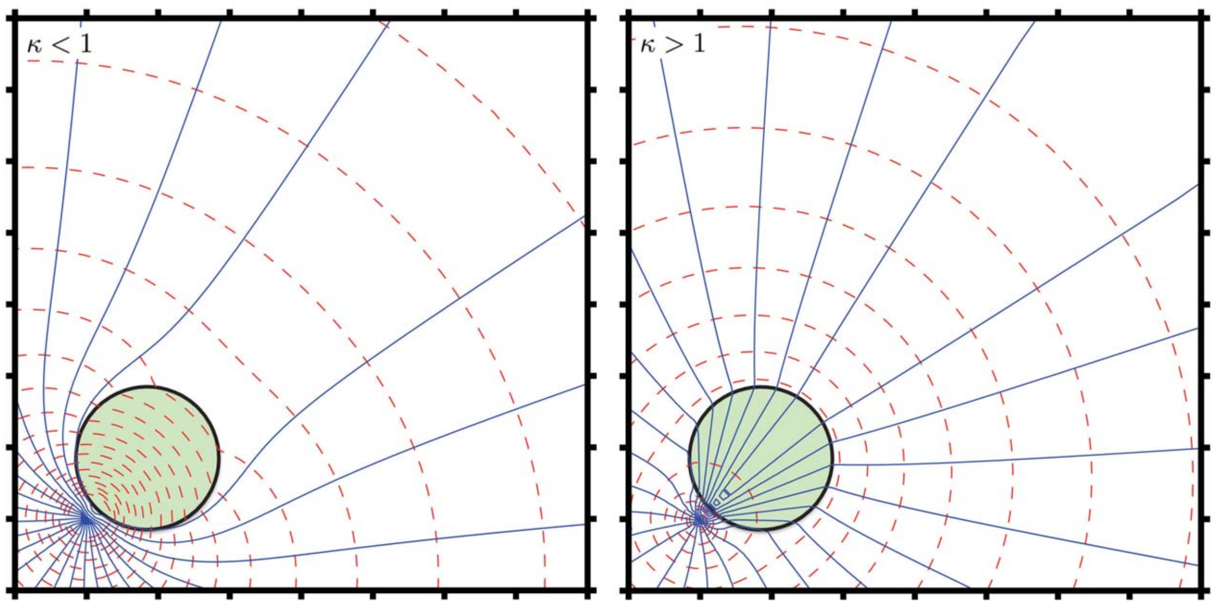

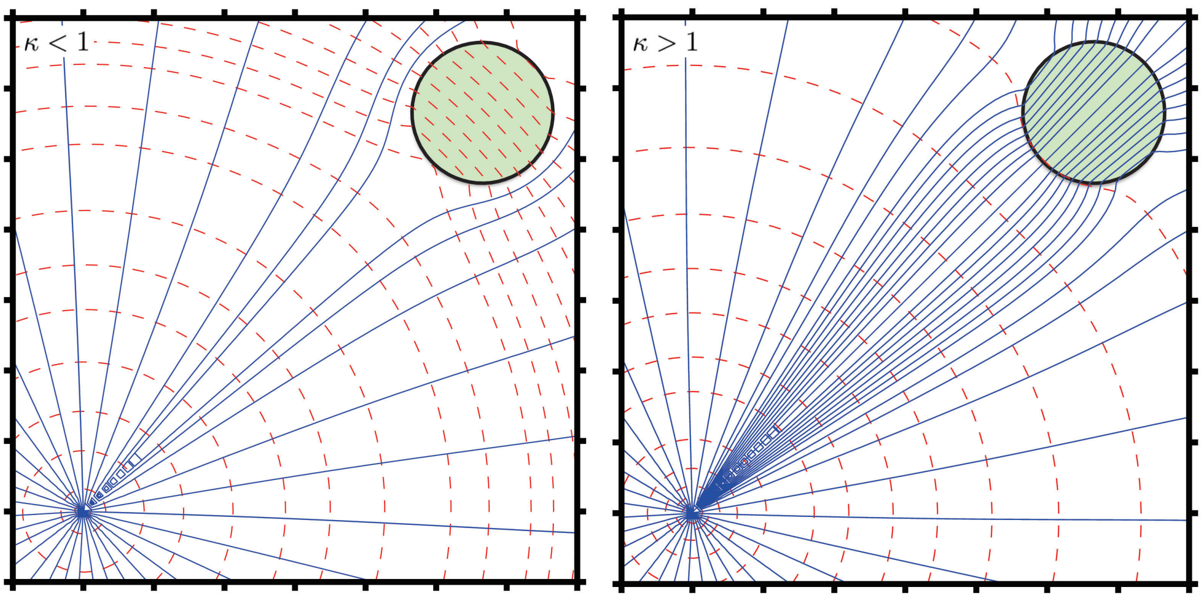
$\kappa < 1$
$\kappa > 1$

Accepted to Phys. Fluids 10.1063/5.0147691

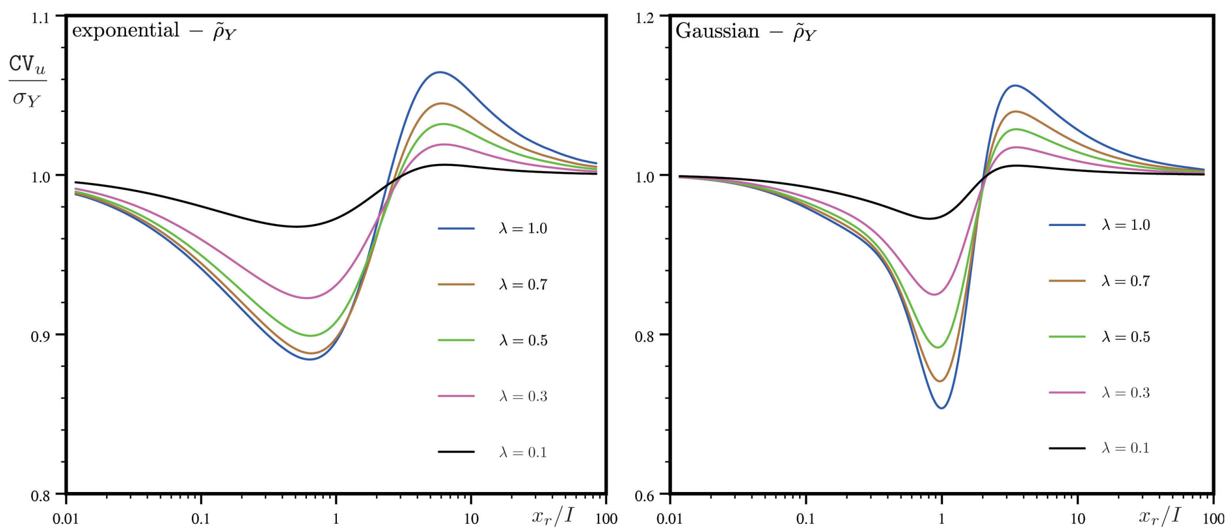

Accepted to Phys. Fluids 10.1063/5.0147691